Science and Technology for Energy Transition **79**, 48 (2024)
© The Author(s), published by EDP Sciences, 2024
https://doi.org/10.2516/stet/2024043

Available online at:
stet-review.org

REGULAR ARTICLE

OPEN ACCESS

A natural hydrogen seep in Western Australia: Observed characteristics and controls

Krista Davies[1,2,*], Emanuelle Frery[1], Ausama Giwelli[1,3], Lionel Esteban[1], Alireza Keshavarz[2], and Stefan Iglauer[2]

[1] CSIRO Energy, 26 Dick Perry Ave, Kensington, Western Australia 6151, Australia
[2] Edith Cowan University School of Engineering, 270 Joondalup Drive, Western Australia 6027, Australia
[3] Currently at INPEX Australia, 100 St Georges Tce, Perth, Western Australia 6000, Australia

Received: 21 May 2024 / Accepted: 5 June 2024

Abstract. Natural hydrogen (H_2) is a promising resource for the energy industry's transition to zero-carbon fuels. However, its extent and feasibility for exploitation remain unclear. A key step towards discovering subsurface dihydrogen accumulations is detecting H_2 seeps. This study presents the first autonomous, multi-gas monitoring of a natural hydrogen seep in Australia, where dihydrogen, carbon dioxide, and hydrogen sulphide were measured together. The research revealed significant H_2 seepage on the Yilgarn Craton in Western Australia, with seasonal fluctuations: high emissions after dry summers and reduced emissions following rainfall due to increased groundwater levels. Groundwater appears to act as a seasonal inhibitor to H_2 seepage through the near subsurface potentially leading to false negatives in soil gas surveys post-rainfall and in low-lying areas. This work provides fundamental data for natural hydrogen exploration and therefore aids in the implementation of a large-scale hydrogen economy.

Keywords: Natural hydrogen, Surface seep, Yilgarn Craton, Soil gas monitoring, Groundwater.

1 Introduction

The reduction of carbon dioxide emissions by 2050 requires the rapid development of alternative clean energy industries [1]. One such alternative is using hydrogen (H_2) produced from renewable resources, producing pure water as the only waste product [2–6].

Manufactured hydrogen is generated by a number of mechanisms such as gasification of coal (black hydrogen), steam reforming of methane (grey hydrogen), pyrolysis of methane (turquoise hydrogen) and electrolysis of water (green, yellow, or pink depending on the power source) [7, 8]. In such cases, the hydrogen acts as an energy carrier for the original energy source. Natural hydrogen is directly produced from a set of geological mechanisms including radiolysis, organic activities, tectonics, and mineral alterations, and is thus a primary energy source. Natural hydrogen has an estimated full lifecycle greenhouse gas intensity of one-third that of green hydrogen [9] making it advantageous for the environment, but also more energy efficient than other forms of hydrogen.

With recent natural H_2 discoveries in Mali [10], France [11], and South Australia [12], exploration has gained strong interest internationally [10, 13–15]. However, natural H_2 exploration is in its infancy and little data is available. Past petroleum wells rarely recorded dihydrogen gas concentrations, making this new field of research challenging.

Detecting dihydrogen surface micro seeps may be an indicator of deeper accumulations, however, yet there are no standard procedures to sample H_2 at the surface. It is therefore critical to standardize exploration techniques for soil gas sampling in the field [16]. Point sampling for natural H_2 in soils has been documented by several authors [17–19], but continuous and long-term studies of natural H_2 seeps are limited to two sites in the Sao Francisco Basin in Brazil [20–22].

Variable H_2 gas emissions were measured from the soil in and around sub-circular depressions in Brazil. These sub-circular depressions may appear as salt lakes and are thought to relate to the occurrence of H_2 in the subsurface [14, 21, 23, 24].

No studies to date have continuously monitored natural H_2 seepage in Australia or have combined long-term H_2 with other trace gases to better constrain the potential source. Additionally, prior to this work, long-term autonomous monitoring has been focussed in and around areas with sub-circular depressions; thus, significantly more research is required to enable efficient natural H_2 exploration and production.

* Corresponding author: krista.davies@csiro.au

This is an Open Access article distributed under the terms of the Creative Commons Attribution License (https://creativecommons.org/licenses/by/4.0), which permits unrestricted use, distribution, and reproduction in any medium, provided the original work is properly cited.

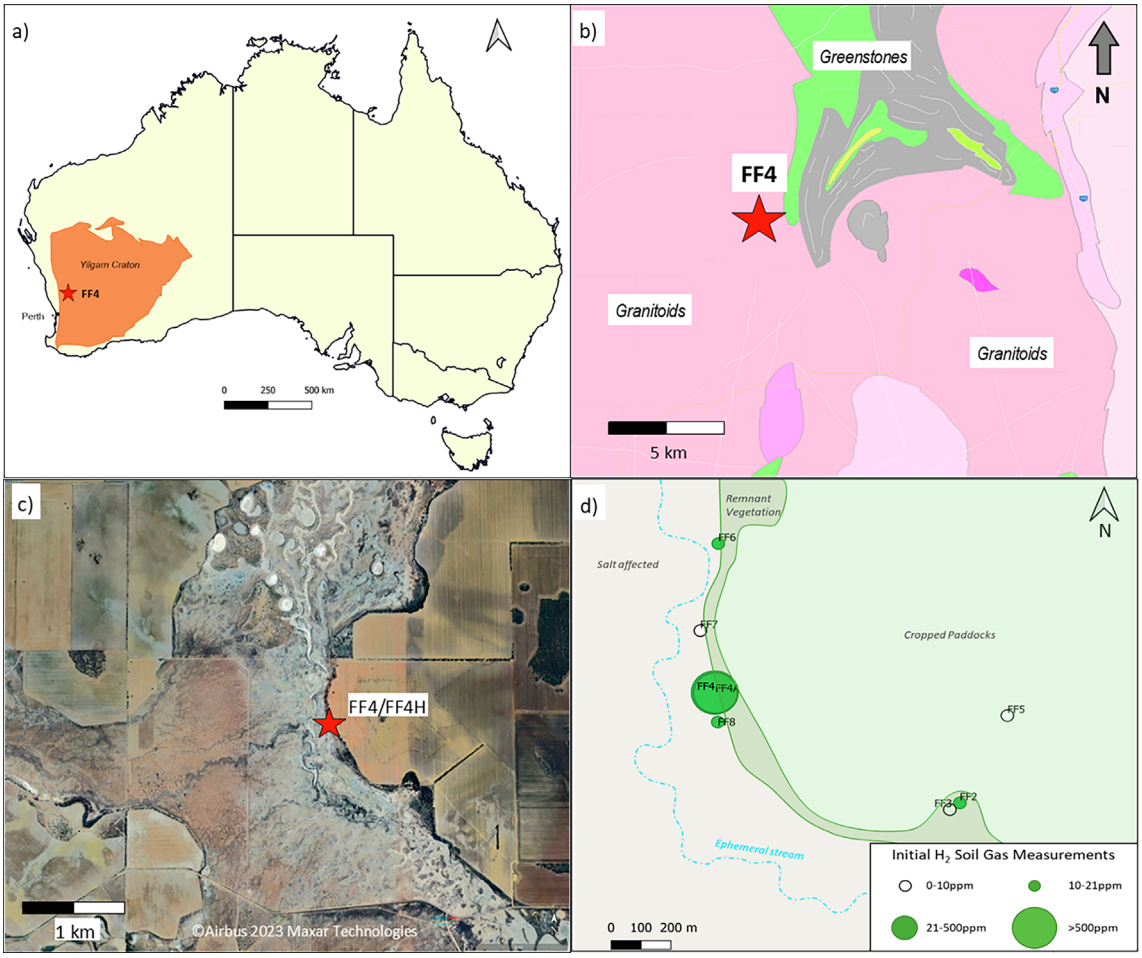

Figure 1. Shows (a): Yilgarn Craton and FF4 Sample location (30°55′39″S, 116°35′35″E). (b) FF4 site interpreted bedrock geology (c) site morphology of ephemeral stream and salt-affected flood plains. Google Earth Image modified after Maxar Technologies, and (d) Results of a regional point soil gas sampling program that identified elevated H_2 concentrations at the FF4 site.

We here present the first long-term monitoring of a natural dihydrogen seep in Australia. In a novel approach, carbon dioxide (CO_2) and hydrogen sulphide (H_2S) were monitored together with H_2, to determine whether associated trace gases could assist in identifying the geologic source. The Yilgarn Craton site represents the first natural H_2 seep identified on the flood plain of an ephemeral stream, as opposed to in and around sub-circular depressions.

We identify the scale and variability of the natural H_2 seepage and discuss potential endogenic, environmental, and climatic controls at the site named FF4 and the implications for exploration. This work therefore advances the natural H_2 energy industry and aids in the development of a low-carbon energy future.

2 Study location and geological context

2.1 Yilgarn Craton

The study area is located on private property on the Yilgarn Craton, in the southwest of the state of Western Australia (Fig. 1a) where bedrock comprises extensive Archean granitoid and greenstone terrains [25–27]. The greenstones comprise metamorphosed basalts, gabbros, chlorite schists, and serpentinites and are interbedded with metamorphosed sediments and banded iron formations [28, 29]. They form arcuate belts of metamorphosed sedimentary and mafic volcanic rocks that lie between the granitoids at the surface and are interpreted to extend to depths of up to 5 km below the study location [30, 31]. Granitoids include granites, tonalites, granodiorites, and Proterozoic sedimentary rocks that overlie parts of the Craton [32, 33]. The Yilgarn Craton comprises an imbricated middle crust, which was subjected to subsequent crustal spreading, reworking, and injection of late plutons via rejuvenated listric faults (Fig. 1d). These reworked faults, imaged on deep seismic data, sole out near the Moho boundary and offer potential deep-seated pathways for fluid migration through the crust [30].

The geomorphology of the study area comprises an ephemeral stream in the centre of an elongated depression, with a wide rim of low-lying salt-affected flat areas for 500 m to 2 km on either side (Fig. 1c). The stream is

Table 1. Measurement ranges and precision ranges of gas detectors used in this study.

		H_2 (ppm)		CH_4 (ppm)		CO_2 (ppm)		H_2S (ppm)	
		Min	Max	Min	Max	Min	Max	Min	Max
WHALI	Range	0	2000			100	20000	0	100
	Precision	10		Not Installed		40		0.6	
EVA	Range	0	2000			100	20000		
	Precision	10		Not Installed		40		Not Installed	
iBrid MX6	Range	0	2000	0	50000	0	50000	0	500
	Precision	1		500		100		0.1	

Sources: [37–41].

slow-flowing and meanders seasonally across the salt pan, causing yearly variations in standing water and soil saturation. The groundwater at the FF4 site was acidic (pH 5.75) and highly saline (77,000 ppm), consistent with previous groundwater studies in the western Wongan Hills locality [34].

Point soil gas monitoring was performed at 15 locations in the area in January 2022, six of the locations were drilled within a 1 km radius including the FF4 site (Fig. 1d). The initial FF4 H_2 concentration measured during point sampling was 800 ppm [35] and the decision was made to conduct more detailed autonomous monitoring at that site in order to prove that H_2 was emitting continuously, and not simply the result of drill bit cataclasis [36], and to better understand the variations in natural H_2 emissions.

3 Methods

3.1 Boreholes

Three boreholes were drilled for the autonomous monitoring to a depth of between 80 cm and 100 cm initially with a 40 mm diameter auger drill bit used to minimize artifact H_2 generation via drill bit metamorphism [36]. Capped PVC tube liners were placed into each borehole comprising a 20 mm diameter PVC pipe. The lower 20 cm of the liner was perforated with 5 mm holes (1 per 2.5 cm^2 spacing). During soil gas measurements, 3 mm PVC tubing was inserted through the tube liner into the perforated interval to draw gas from the base of the hole (80–100 cm below the surface).

3.2 Gas detection

3.2.1 Point sampling

Gas was detected during the initial point sampling survey by a handheld iBrid MX6. The iBrid MX6 gas detector was fitted with H_2, CO_2, methane (CH_4) and H_2S sensors. Measurement ranges and precisions of the sensors are shown in Table 1. The iBrid MX6 is fitted with an internal pump that pumps gases across the sensors at a rate of 300 ml per minute and was calibrated prior to each survey period.

3.2.2 Autonomous sampling

Two stationary autonomous multi-gas detectors (Axiom Sensing; WHALI & EVA, origin: Australia) were used in this study.

The pumped autonomous logging unit (Axiom Sensing; WHALI, origin: Australia) was equipped with H_2, CO_2, and H_2S sensors, temperature, and pressure sensors, and a peristaltic pump capable of pumping gas vapors at 300 ml per minute, similar to the iBrid MX6. The range of the H_2 detector was 0–2000 ppm, with a precision of 10 ppm (Table 1). Automatic measurements were made for 3 min either every 15 or 30 min.

The autonomous unit was deployed at the FF4 site for 5 h on 20th February 2022, 7 days from the 23rd to the 30th of April 2022, and 7 days from the 9th to the 16th of February 2023.

The pumped autonomous WHALI unit shut down after five hours on the first day of operation (20th February 2022) due to groundwater intrusion. A water management system was subsequently added and used during April 2022 and February 2023 to evacuate and dispose of groundwater drawn through the system while pumping soil vapors to the sensors (Fig. 2).

In April 2022 the FF4H site was selected for the autonomous sampling, located 8 m up-dip from the original FF4 site, which was inundated with water. An initial H_2 concentration of 47 ppm was measured at FF4H with the handheld MX6 gas meter.

The site was inaccessible from July to November, and upon returning in November 2022, measured trace gas concentrations in the air space above the standing water in the boreholes were consistent with air, with no H_2 detected [35].

In February 2023 the original FF4 borehole was chosen for the autonomous sampling.

A second autonomous, passive measurement system, *i.e.* non-pumped (Axiom Sensing; EVA, origin: Australia,) was also deployed at the FF4 site during February 2023 approximately 80 cm away from the WHALI unit to compare the results of the two systems. The passive system was not available prior to that time.

As both autonomous units sit above ground, and electrochemical sensors are sensitive to temperature variations, all H_2 concentrations (cH_2) and hydrogen sulphide concentrations (cH_2S) results displayed herein represent

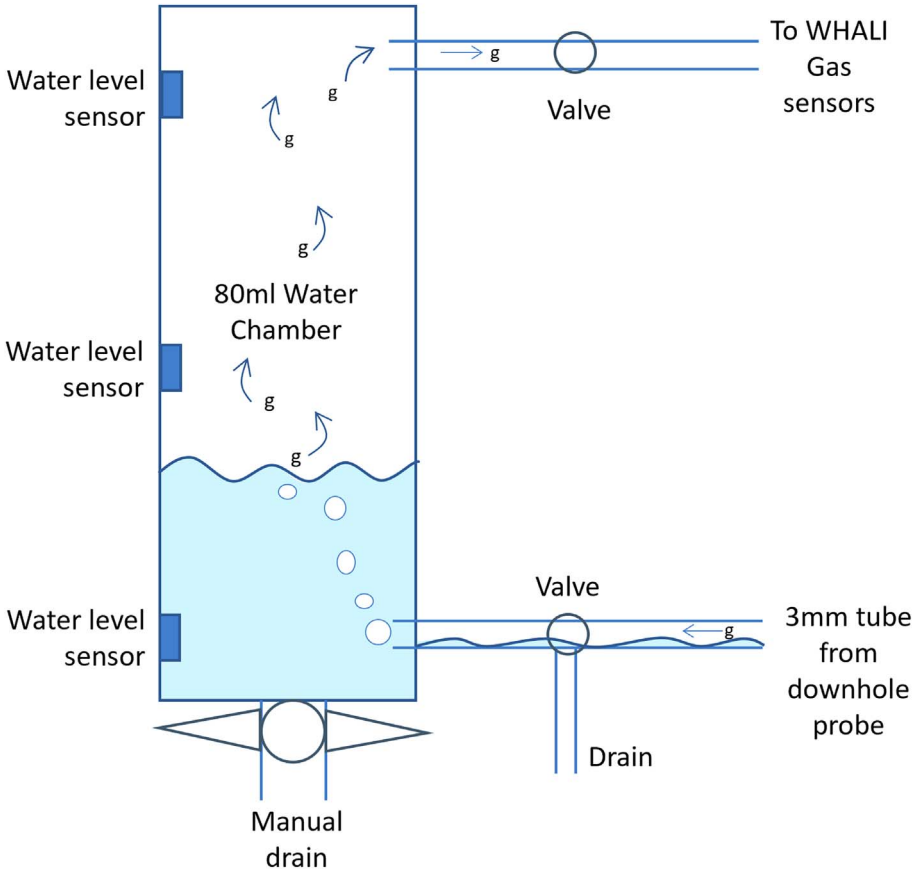

Figure 2. WHALI Autonomous Water Management System.

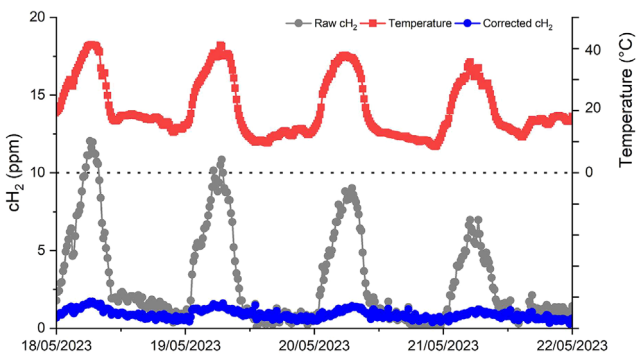

Figure 3. Sensor reaction to temperature (red) while measuring air, showing raw H_2 concentration measurement (grey) and temperature-corrected H_2 concentration measurement (blue). The dotted line shows the lower accuracy of the sensor of 10 ppm.

temperature-corrected concentrations according to the manufacturer's specifications [40]. The following polynomial equation has been applied:

$$y = x\left(\frac{1}{(0.0006z^2) + (0.0165z) + 0.5}\right) \quad (1)$$

x = Raw concentration
y = Temperature corrected concentration
z = Measured temperature at sensor

Figure 3 shows the results of test measurements in air ($H_2 < 1$), which were recorded for two minutes every 15 min over a four-day period, where the temperature at the sensor ranged from 8.5 °C to 41 °C. The raw H_2 concentrations represent the maximum recording during each two-minute sampling period. Equation (1) was applied to generate the temperature-corrected H_2 concentration. This shows the extent of the sensor reaction due to temperature variation at a peak of 41 °C was 12 ppm, which corrected to 2.5 ppm. As the accuracy of the sensor in the autonomous units is 10 ppm, <10 ppm is insignificant. Therefore, the cH_2 measured can be effectively corrected with the temperature correction equation. The CO_2 sensors are infra-red sensors with internal thermometers and self-calibration, and thus CO_2 concentrations do not require environmental correction.

4 Monitoring results

4.1 H_2 concentration

Normal cH_2 in air is <1 ppm, therefore, $cH_2 > 1$ ppm indicates H_2 seepage. However, as the autonomous monitoring unit had an accuracy of 10 ppm, for this study we consider >10 ppm as significant. Here $cH_2 >> 10$ ppm was measured

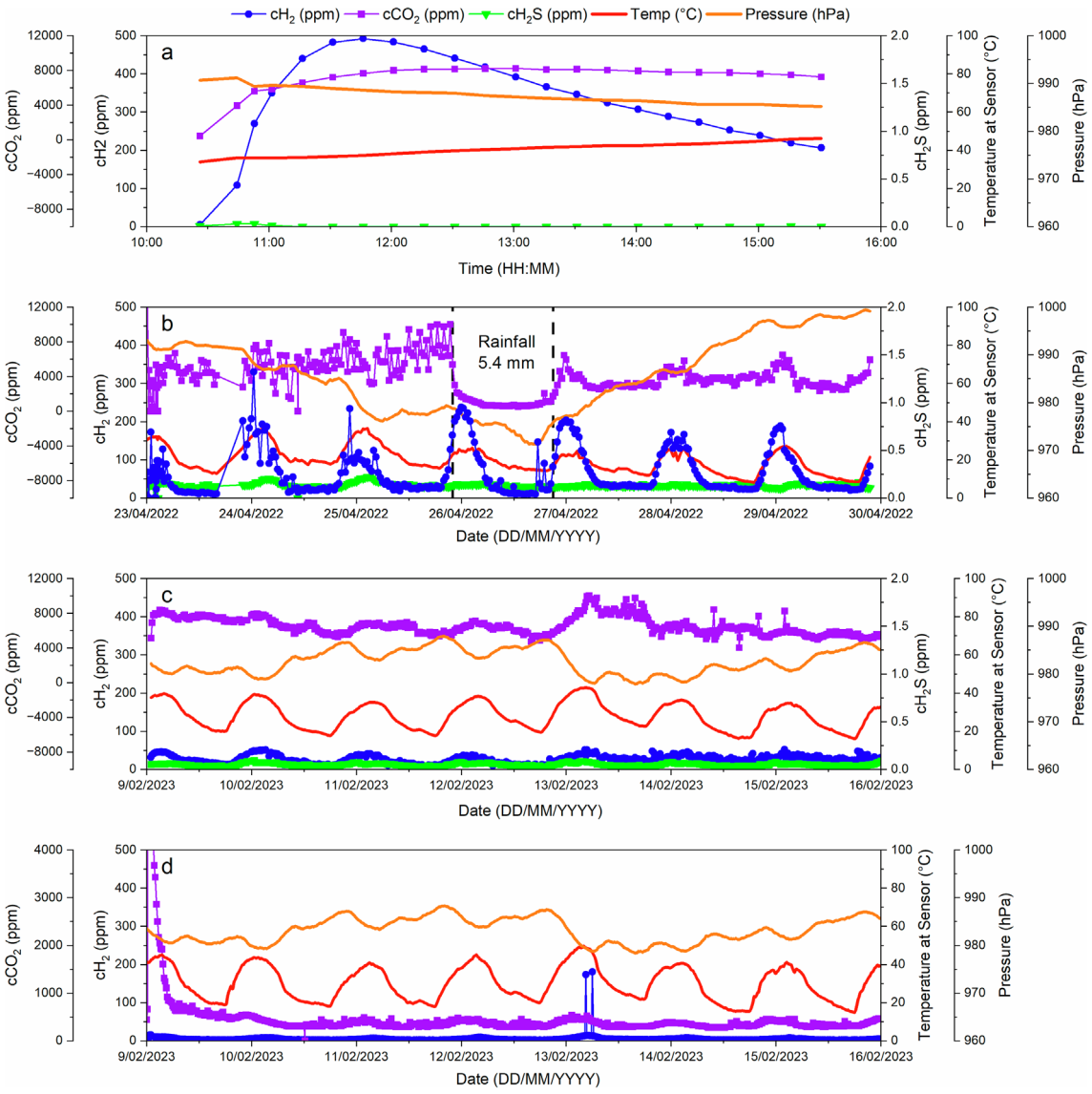

Figure 4. Gas concentrations of H_2, hydrogen sulphide, and carbon dioxide plus atmospheric pressure and temperature measured at the sensor from the FF4 site (a) WHALI – 20th of February 2022, installed immediately after drilling of the FF4 hole (b) WHALI – 23rd of April to the 30th of April 2022 (c) WHALI – 9th to the 16th of February 2023 and (d) EVA – 9th to the 16th of February 2023.

at FF4 during all three monitoring periods (February 2022, April 2022, and February 2023 (Fig. 4).

The amplitude of the H_2 concentrations varied strongly between monitoring periods, despite similar temperature and pressure conditions in the summers (February) of 2022 and 2023 (Table 2). In February 2022 a maximum cH_2 of 493 ppm was measured (average 326 ppm), while the highest cH_2 for April 2022 was 330 ppm (average 62 ppm) and the peak cH_2 was 52 ppm (average 26 ppm) for February 2023 (WHALI). The peak cH_2 measured by the EVA system in February 2023 was 180 ppm, but the average (4 ppm) was insignificant.

A diurnal bell-shaped trend was established during monitoring in April 2022 and February 2023, with the highest cH_2 measured in the middle part of the day and the lowest cH_2 in the evenings.

4.2 Carbon dioxide concentrations

The carbon dioxide concentrations (cCO_2) measured across the monitoring periods ranged from 442 to 15,558 ppm (Table 2), indicating valid soil gas measurements. In February 2022, very high and stable cCO_2 was measured across the limited monitoring period. For the first week of April 2022 monitoring period, the cCO_2 concentrations were high, irregular, and gradually increasing. A more regular oscillating pattern was observed in the second half

Table 2. Peak gas concentrations and atmospheric conditions measured during the three monitoring periods in the WHALI autonomous unit.

		WHALI unit			EVA unit
		February 2022*	April 2022	February 2023	February 2023
H_2 (ppm)	Range	5–493	0–330	5–52	1–180
	Average	326	62	26	4
	Standard Dev.	124	58	10	9
CO_2 (ppm)	Range	442–8233	499–15,558	1697–10,023	279–7570
	Average	7088	3815	6487	436
	Standard Dev.	1781	2205	1018	518
H_2S (ppm)	Range	0–0.05**	0–0.4**	0–0.24**	–
	Average	0.01**	0.1**	0.05**	–
	Standard Dev.	0.01**	0.1**	0.04**	–
Temperature (°C)	Range	34–46	8–36	16–43	14–49
	Average	40	21	28	29
	Standard Dev.	4	7	7	9
Pressure (hPa)	Range	985–991	971–999	977–990	977–990
	Average	988	986	984	984
	Standard Dev.	2	8	3	3
Groundwater Extracted (ml)	Total for 7 days	–	20,299	30,087	–
	Range per sample	–	0–375	0–196	–

*February 2022 monitoring was limited to a 5-h period. **Below resolution of sensors.

of the April 2022 monitoring period and in most of February 2023.

cCO_2 peaked on the EVA unit in February 2023 at 7570 ppm an hour after installation along with a cH_2 of 16 ppm. Other than the two cH_2 peaks on the 13th of February 2023, concentrations did not reach those levels again. This may have been due to soil gas readings reaching the sensors before the borehole became inundated with groundwater.

4.3 Hydrogen sulphide concentrations

Hydrogen Sulphide concentrations (cH_2S) were insignificant, measuring below the 0.6 ppm precision of the H_2S sensors (Table 1, Table 2). This result varies from the headspace gas analysis conducted at the site between November 2022 and February 2023, where cH_2S up to 31 ppm (average 3.4 ppm) was detected with vigorous agitation of the groundwater samples [35]. Hydrogen sulphide is slightly soluble in water, but solubility decreases with increasing salinity [42]. This suggests that gaseous H_2S may be held within the groundwater, with degassing requiring vigorous agitation, rather than the gentle water movement created through the WHALI water management system.

4.4 Methane concentrations

Methane was measured during initial point sampling at the site in early February 2022 but was not measured by the autonomous units during continuous monitoring. Five measurements were taken using the handheld iBrid MX6 at the FF4 site on the 7th and 8th of February 2022 and measured methane concentrations from 0 to 4500 ppm. Headspace gas analysis of groundwater samples at this site between November 2022 and February 2023 measured methane concentrations from 0 to 6500 ppm [35].

4.5 WHALI pumped vs EVA passive autonomous unit

The average cH_2 for the EVA system was approximately one-quarter to one-fifth of the cH_2 measured by the WHALI system at the same time. Because the WHALI system is pumped, it draws a sample of 600–900 ml of soil gases over the sensors, which is derived from the area around the borehole.

Alternatively, the EVA system relies on whatever volume of soil gases migrate up the borehole to the sensor. If there is standing water in the borehole, soil gases must break through the interfacial tension of groundwater to rise to the sensors at the surface.

cCO_2 measured by the pumped WHALI unit was approximately ten times that measured the passive EVA unit. The exception to this was one hour after both units were emplaced on the 9th of February 2023, when measurements were similar. This may have been due to there being no water saturation in the borehole for the initial part of that day. Again, the main difference is likely to be the pumping. As CO_2 is significantly heavier than H_2, a larger concentration differential is required for the gas to migrate up the borehole, compared to lighter H_2.

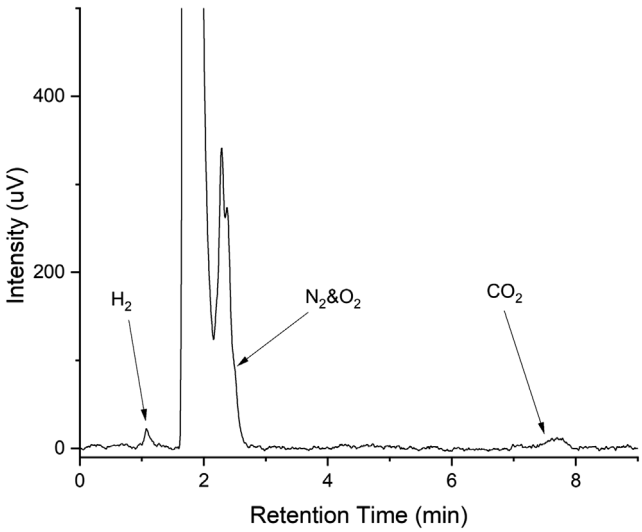

Figure 5. Gas Chromatogram of sample FF4 from 19th April 2024. cH_2 measured 530 ppm and cCO_2 measured 1160 ppm.

4.6 Groundwater volumes

We measured groundwater volumes extracted from the WHALI unit over the April 2022 and February 2023 autonomous monitoring periods. The total groundwater extracted during the seven-day monitoring periods in April 2022 and February 2023, was 20.3 L and 30.1 L, respectively (Table 2). While a greater total volume of water was extracted in February 2023, the largest volume of water extracted during a single monitoring cycle occurred in April 2022. Thus, groundwater levels fluctuated during April 2022, whereas by February 2023 the groundwater saturation was consistently high.

4.7 Gas samples

Gas Samples were collected from the FF4 site during August 2023 and April 2024, in order to confirm the H_2 gas emitting from the boreholes, as detected by the handheld gas sensors and autonomous sensors. The samples confirmed cH_2 in soil gas from the FF4 site. The maximum cH_2 measured from gas samples was 300 ppm (August 2023) and 530 ppm (April 2024) (Fig. 5).

5 Discussion

5.1 Soil gas transport mechanisms

Diffusion and advective pressure pumping are the two fundamental processes governing the gas exchange between soils and the atmosphere [43–46]. Diffusion occurs as gases naturally move from areas of high concentration to low concentration, driven by concentration gradients [47, 48]. This process is slow but operates over short distances, allowing gases to permeate through the soil matrix. The diffusion of gases through soil is influenced by physical parameters such as the density of the gases; atmospheric pressure; total porosity; soil moisture; permeability and fractures facilitating preferential flow [46, 47, 49].

Advective pressure pumping involves the movement of gases due to pressure differentials within the soil. This can be caused by wind, temperature and atmospheric pressure gradients, leading to the displacement of gases through soil pores [43, 45, 50, 51].

5.2 Climatic and environmental controls

5.2.1 Temperature

Diurnal H_2 emissions occurred at FF4, where cH_2 fluctuated in a bell-shaped pattern, peaking in the middle of the day, and falling to low levels during the cooler evenings (Fig. 4). While cH_2 and temperature are correlative on a daily scale, Figure 6a shows that there was no overall significant relationship between cH_2 and temperature measured at the sensor.

Soil temperatures influence diffusive gas movements through soil and fluctuate both with depth and seasonally due to factors such as solar radiation, air temperature, soil moisture content, and the thermal properties of the soil itself [52, 53]. The influence of air temperature and solar radiation on soil temperature is highest close to the surface, and diminishes with increasing depth [53]. Cheng *et al.* [52] demonstrated modest seasonal variation in soil temperature at 80 cm in the low-latitude plateau of China (15–23 °C range), but minimal diurnal variation. Zeng *et al.* [54] found, that in arid climates, diurnal temperature variations can penetrate soils down to 1 m depth, but the hourly temperature gradient variation was low (0–0.5 °C).

The soil gas in this study was drawn from 80 cm to 1 m below the surface, where soil temperatures would be expected to vary seasonally, but not significantly on an hourly basis. Therefore, we can assume that in the summer and autumn months, the soil temperature is higher, enabling increased diffusive flow of all gases. However, soil temperature cannot account for the diurnal flux of cH_2 observed in all cases or the diurnal pattern observed in CO_2 following the precipitation event on the 26th and 27th of April 2022.

The average ambient temperatures, average cH_2 and average cCO_2 were all highest during the February 2022 monitoring. February 2023 had the next highest temperatures and average cCO_2, but the lowest average cH_2. This suggests a difference in the main transport mechanisms of CO_2 and H_2 through soils. The average CO_2 concentrations appear to follow the seasonal variations in soil temperature, suggesting the primary mechanism of CO_2 transport may be diffusion.

While the diurnal H_2 variations appear to trend with temperature on a daily time frame, this relationship appears to be correlative rather than causal (Fig. 6a).

The diurnal patterns observed at FF4 are consistent with those documented at the Sao Francisco site in Brazil [22]. In that case, the authors suggested that while there was a correlation between temperature and cH_2, it was coincidental, as the temperature did not vary significantly below 0.5 m depth. Rather, they postulated a

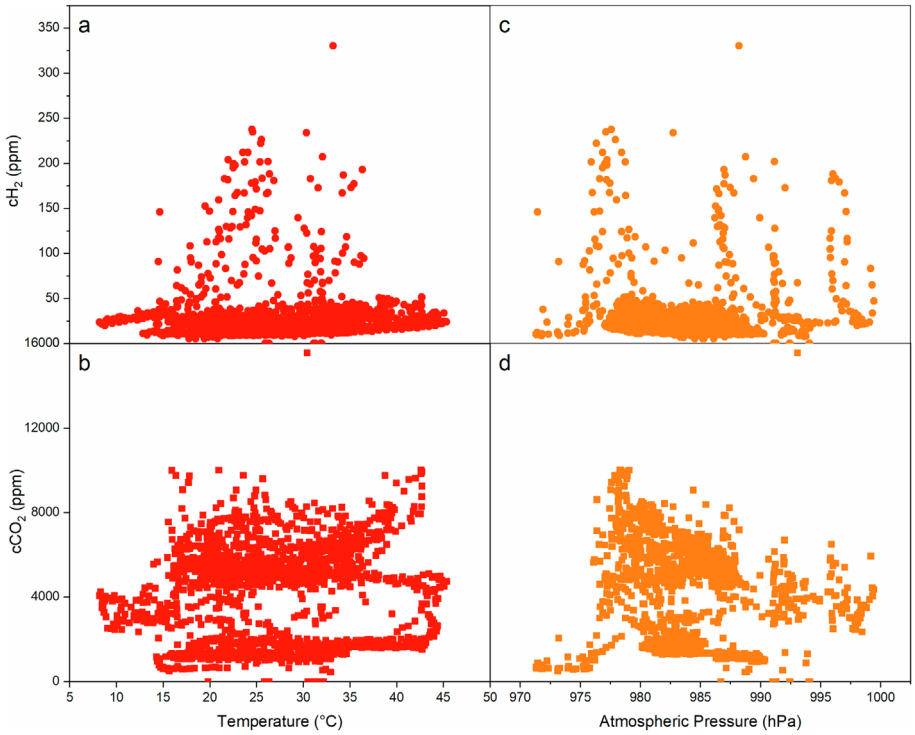

Figure 6. All data from autonomous monitoring periods April 2022 and February 2023 (a) cH_2 vs temperature (b) cCO_2 vs temperature (c) cH_2 vs pressure and (d) cCO_2 vs pressure.

relationship between atmospheric pressure and near-surface gas transport with a lag between the decreasing atmospheric pressure and subsequent increase in cH_2 [20, 22].

5.2.2 Pressure

Overall, cH_2 and cCO_2 varied substantially across pressure conditions (Fig. 6c & d), suggesting that absolute atmospheric pressure is not a predictor of the amplitude of the cH_2 or cCO_2. This suggests that an alternative control, such as advection from deep in the sub-surface, or bacterial activity controls the amount of cH_2 in the soil. However short-term relationships were seen and are discussed further here.

On the 13th of February 2023, a large pressure drop was observed on both the WHALI (Fig. 4c) and EVA (Fig. 4d) units. Following the pressure drop, two large H_2 peaks were measured on the EVA system (178 ppm and 180 ppm) and corresponded to the highest cH_2 measurement on the WHALI system (52 ppm) for February 2023. The difference in reaction by the two systems is deduced to be the difference in sampling methods. The passive EVA system does not draw water but relies on passive flux. We propose the large pulse was the result of the H_2 gas pressure building up before overcoming the interfacial tension and forcing through the groundwater to the sensor [55]. In contrast, the pumped WHALI system consistently detected the elevated cH_2 over several hours, dispersed within the groundwater, by agitating the sample through the water management system (Fig. 7).

cH_2 exhibited diurnal flux throughout all periods of monitoring at the FF4 site. cCO_2 followed a subdued diurnal flux pattern after the rainfall event of the 26th to 27th of April, and throughout the February 2023 monitoring period (on both the pumped WHALI unit and the passive EVA unit). The diurnal pattern is consistent with measured daily drops in pressure (Fig. 4). A similar diurnal flux pattern of cH_2 has been documented in Brazil [20, 22, 56, 57], and diurnal CO_2 flux is well known, although for the latter samples depths are usually shallower and therefore more affected by ambient temperatures [58–63].

In both the April 2022 and February 2023 campaigns, small dips in pressure coincided with the peak diurnal H_2 concentration (Fig. 8).

The process of pressure pumping (changing barometric pressure causing upward and downward mass flow of soil gases) as a mechanism for soil gas transport is well known [22, 43–47, 50, 61, 63–65]. Gases of different densities react differently to pressure pumping [46]. High density gases such as CO_2 are less sensitive to pressure-induced advection, whereas low-density gases such as Helium, are highly reactive to pressure-induced advection [43, 44, 46, 64].

We propose that the strong diurnal flux observed in the cH_2 trend is the result of the low density di-hydrogen molecule reacting to barometric pressure pumping similar to the behaviour of Helium in soil gas [43, 64]. Figure 8 shows temperature and pressure plots for the April 2022 monitoring period, with both plots coloured according to cH_2. As pressure falls in response to ambient temperature increase, the H_2 concentrations increase. The asymmetry of the H_2 con-

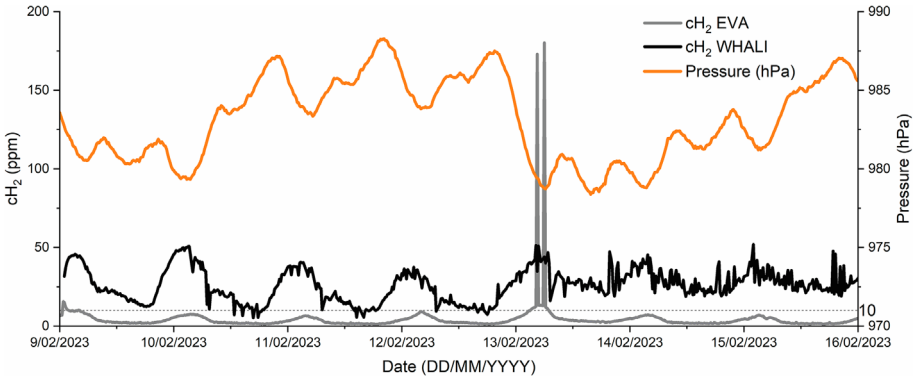

Figure 7. cH_2 for the WHALI and EVA autonomous logging units for the February 2023 monitoring period, with atmospheric pressure. Dotted line shows the lower accuracy limit of the H_2 sensors.

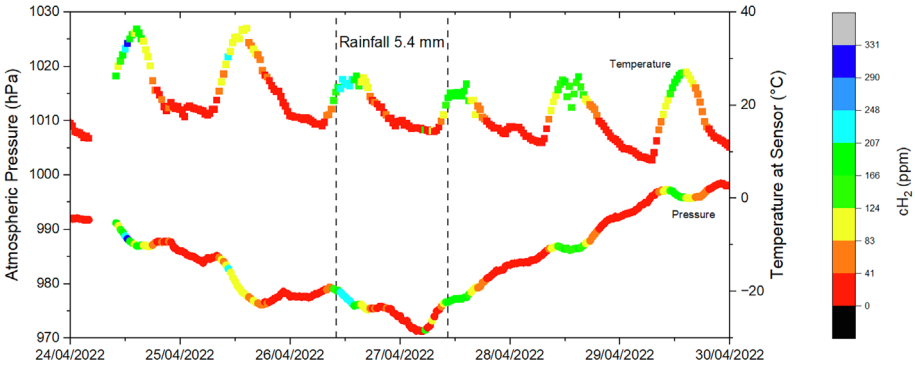

Figure 8. Temperature (upper squares) and Pressure (lower circles) measured at the site FF4 from the 24th to 29th April 2022. Both graphs are coloured by cH_2 (ppm) where blue is high and red is low.

centration with temperature confirms the flow of gas through the subsurface is controlled by pressure, but the daily barometric pressure change is related to temperature, hence the appearance of cH_2 to trend with ambient temperature.

Thus, while neither pressure or temperature control the absolute H_2 soil gas concentrations in the soil, atmospheric pressure appears to enable the movement of H_2 to the surface on a diurnal basis through pressure pumping.

5.2.3 Groundwater levels and soil moisture

Groundwater volumes extracted by the WHALI water management system were measured in April 2022 (20.3 L) and February 2023 (30.1 L). The highest cH_2 measured at FF4 in this study occurred during February 2022, when no water had yet inundated the borehole. Following this, the next highest concentrations occurred during April 2022 when there was moderate groundwater extraction. During February 2023, H_2 concentrations were consistently and significantly lower than the previous monitoring periods while overall water volume extraction exceeded the April 2022 monitoring period by 48%.

Water levels in boreholes varied substantially between campaigns due to the higher levels of rainfall in the preceding months (Fig. 9). Rainfall was measured by the Bureau of Meteorology at the Wongan Hills Weather Station #08137, located 13 km northeast of FF4 [34]. High rainfall in the second half of 2022 led to high groundwater levels [34], and saturated salt lakes in the region throughout the summer of 2023 (Fig. 10). There was a strong negative correlation between the six months rainfall before each monitoring period (BOM, 2023), and cH_2 (Fig. 9). Thus, when no water was initially observed in the FF4 borehole (summer season 2022), peak cH_2 was 493 ppm; however, as the groundwater at the FF4 site rose following significant rainfall the H_2 concentrations reduced.

In Sao Francisco, Brazil, the centres of circular depressions, which were described as flood zones, measured lower H_2 emissions to surface than the surrounding dry areas [21].

The reason for the apparent inhibition of cH_2 flow in moist soils may be due to either higher bacterial consumption in groundwater, or the physical inhibition of H_2 diffusion.

The interfacial tension between H_2 and H_2O is high at ambient conditions, and diffusivity at surface conditions of dihydrogen in water is close to zero [55]. Therefore, porous water-wet rocks, and even water itself, can form an impermeable seal for H_2 gas [10, 55, 66].

Experimental studies by [67] showed significantly lower H_2 diffusion rates through water and brine saturated

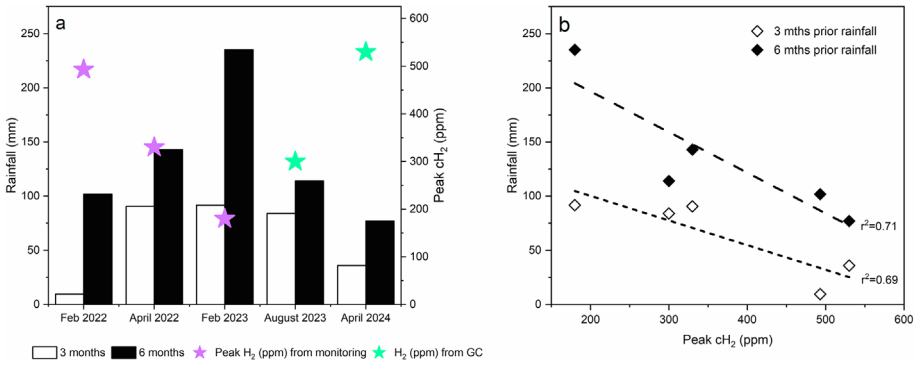

Figure 9. (a) Rainfall preceding the monitoring periods at FF4, compared to the highest cH_2 from the WHALI autonomous monitoring unit during the monitoring periods Feb 2022, April 2022 and February 2023, and cH_2 measured via gas chromatography from gas samples taken at the FF4 site. (b) Rainfall preceding the monitoring periods at FF4, compared to the highest cH_2 from the WHALI autonomous monitoring unit and measured from gas samples. Pearsons coefficient is higher for the cH_2 vs previous 6 months rainfall compared to cH_2 vs previous 3 months rainfall.

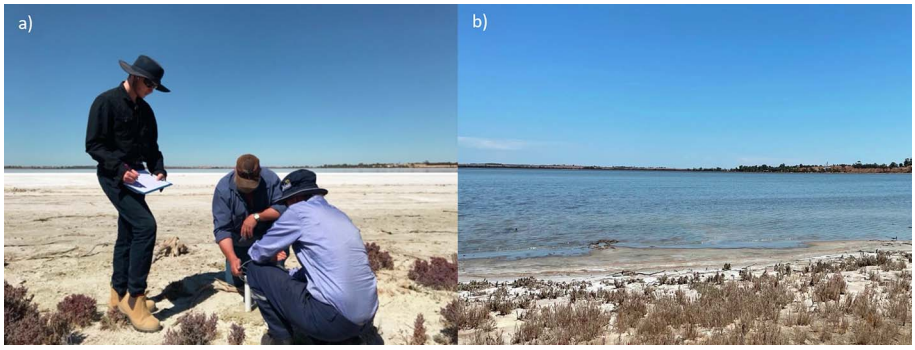

Figure 10. A nearby ephemeral salt lake shows very little standing water was present during (a) January 2022 compared with (b) February 2023.

sedimentary rocks as opposed to dry samples, and higher diffusion rates through sandstones vs claytones. A similar relationship can be expected in soils, where diffusion rates will be lower in brine saturated samples, and indeed is supported by the results of this study. [68]

Davies *et al.* [35] demonstrated that high concentrations (up to 1684 ppm) of natural H_2 was trapped in groundwater and degassed into the headspace of a measurement vessel when agitated vigorously. In this study, the WHALI water management system (Fig. 2), provided significantly less agitation and cH_2 concentrations measured were lower. The high levels of H_2 liberated during headspace gas analysis by [35] suggest that physical inhibition, rather than bacterial consumption, is responsible for the reduced H_2 soil gas emissions measured at the FF4 site during periods of high groundwater.

We propose that during periods of low groundwater levels, H_2 can migrate through the subsurface via feeder systems such as fault zones into the dry soil where it flows to the surface. Conversely, when groundwater levels rise, H_2 diffusion into surface soils may be impeded by water at the terminus of the conduit fault, trapping H_2 in groundwater and preventing its fast movement to the surface.

Soil moisture is known to impact the movement gases through soils as it reduces the porosity [46, 47, 69–71] and CO_2 emissions are lowest when groundwater levels are closest to the surface [72].

While soil moisture was not monitored in this study, we use rainfall as a proxy. During the April 2022 monitoring period, CO_2 emissions were high and generally increasing for the first three days. cCO_2 dropped dramatically when the rainfall occurred on the 26th of April, and thereafter adopted a subtle diurnal pattern similar to cH_2. We surmise that rainfall increased soil moisture, which decreased the soil temperature and free air porosity, leading to a drop in diffusive CO_2 flux. The diurnal pattern which follows suggests that pressure pumping may be the dominant mechanism of transport for heavier gases only in moist soils [46, 63].

This study demonstrated that groundwater impeded the natural H_2 flow to the surface. Such inhibition may lead to false negative readings in soil gas surveys after high rainfall and in low-lying areas. Alternative exploration methods should be considered in such wet areas.

5.3 Natural hydrogen source

Understanding the source rocks for natural H_2 can de-risk exploration, by focussing efforts on areas with the most conducive geology. This study aimed to advance understanding through continuous monitoring of multiple gases at the surface. Gas analysis techniques such as isotopic analysis may help to characterize the natural H_2 source rocks and are planned for future studies. While isotopic analysis was outside of the scope of the existing study, we may still postulate the most likely sources with the continuous monitoring data available. Five natural H_2 generation mechanisms are possible at the FF4 site, namely radiolysis, water interactions with iron-bearing minerals, mantle flux, gas release from fluid inclusions, and/or bacterial activities [17, 73–75].

5.3.1 Bacterial source

Bacterial community abundance has been shown to be at its highest in the 5–10 cm zone below surface and reduce at depth [76–78]. The soil gas measured during this study was taken from 80 cm to 1 m below surface, at which depth microbial abundance is low [76, 78].

CO_2 and H_2S are classical by-products of bacterial fermentation [72, 79–83]. If the H_2 was produced by bacteria, elevated concentrations of cH_2S and cCO_2 would be expected, and correlate with cH_2. Such patterns were not observed at FF4 where cH_2 and cCO_2 did not correlate (Table 2), and cH_2S was <0.4 ppm during autonomous monitoring.

While further bacterial soil studies are required to verify the microbial influence on the H_2 emissions, the depth of sampling combined with the observed trace gas mixtures suggest that bacterial fermentation is not the most likely source of H_2 at the FF4 site.

5.3.2 Iron-rich minerals and water interactions

The interaction between iron-rich minerals and water, potentially generates H_2 in the ultra-mafic greenstone belt adjacent to FF4, which projects several kilometres into the subsurface [30, 31]. Geochronological data suggest deformation of the Yilgarn Craton greenstone belts around 2.8–2.6 billion years ago [84–86]. However, it remains uncertain whether mafic minerals of this age actively produce H_2 or have fully reacted. Similarly, the permeability of these formations and their ability to allow water penetration crucial for H_2 generation, as well as the release of H_2 to adjacent formations, are unknown.

Studies indicate gas vents above ophiolite belts in various regions produce H_2 created by serpentinization, along with high methane volumes [87–89]. However, methane measured at FF4 comprises less than 0.65% of soil gas volume [35].

Serpentinization and low-temperature iron oxidation typically produce highly alkaline fluids with a pH of 9–12 [89–91], and consistent generation of H_2 gas occurs at pH 8.5 and above [92]. As the groundwater at FF4 is acidic (pH = 5.75), the H_2 generating system would need to be separated from the FF4 groundwater via a perched water table, which seems unlikely as it would impede H_2 migration into the groundwater system. For these reasons, serpentinization is not the preferred mechanism for the H_2 produced at the FF4 site.

5.3.3 Mantle flux

The volatile elements of the earth's mantle are predominantly H_2, carbon, nitrogen, noble gases and sulphur [93]. Those elements are vented as volcanic gases; water vapor, CO_2, SO_2, CO, H_2S and H_2 at the surface [94–96]. The acidic groundwater at FF4 is consistent with a deep mantle-derived fluid source [96], into which abundant CO_2 is dissolved [97].

CO_2 constitutes ~10–49 mol% of volcanic gas emissions [94, 98]. However, the cCO_2 at FF4 were significantly lower (Table 2), ranging from 442 to 15,558 ppm (0.04–1.56 vol%); consistent with cCO_2 in natural soils [99].

Based on these observations, it appears that mantle flux is not the most likely source for the FF4 H_2 seep; however, a full-scale geo-chemical analysis should be conducted before dismissing this potential source mechanism including isotopic analysis of CO_2 and noble gases including helium. Such analysis was outside the scope of the current study but is planned for future work.

5.3.4 Fluid inclusion release

H_2 gas is known to have been trapped in Precambrian granites worldwide, and the Archean granitoids of South and Western Australia have some of the highest H_2 concentrations measured [75, 100].

H_2 may be released from fluid inclusions by heating to ≥600 °C or by mechanical crushing [100, 101]. On the Yilgarn Craton, extensional faulting extends 30–35 km into the lower crust [30, 102]. These faults may provide conduits for migration of gases deep in the crust. Magneto-telluric surveying of the Yilgarn Craton shows zones of high conductivity stretching from the Moho to the near surface, supporting the theory of fluid migration through faults [103, 104].

Heat flow modelling predicts a geothermal gradient of ~18 ± 2 °C km^{-1} over the Yilgarn Craton [105], such that granitoids in the lower crust at 30 km depth exist at temperatures of ~565 ± 60 °C. At such temperatures, H_2 may exsolve from fluid inclusions in the lower crust, contributing a volumetrically significant amount of H_2 into the subsurface.

The juxtaposition of listric faults extending into the lower crust and the endogenic conditions necessary for the release of H_2 from fluid inclusions into these migration conduits provides the ideal geological conditions for the H_2 source at the FF4 site.

5.3.5 Radiolysis

In radiolysis, H_2 is produced by dissociation of groundwater molecules due to radiation from the decay of radioactive isotopes [100, 106–110].

Granites and granitoids have the highest radiogenic heat flow of all rocks, due to their relative abundance of radioac-

tive isotopes (^{40}K, ^{232}Th, ^{235}U, and ^{238}U) [111]. Global studies show that Australia has some of the most radiogenic granites in the world, averaging at 3.53 $\mu W/m^3$, and that the Archean granites of Western Australia are anomalously high, producing up to 9.73 $\mu W/m^3$ [111]. The basement rocks of the Wongan Hills area are well documented through mineral drilling and surface mapping, and comprise granites, granodiorites, tonalites and monzonites [30, 32, 86, 112].

Water radiolysis also produces hydronium ions resulting in the formation of temporary acidic pH spikes in the irradiated groundwater [113]. Flowing groundwaters may retain an acidic signature, consistent with the low pH of the groundwaters at the FF4 site.

The Archean basement lithologies combined with the acidity of the groundwater support radiolysis as a potential source for the natural H_2 observed at FF4.

6 Conclusions and implications

Natural H_2 has the potential to revolutionize the energy industry by enabling zero-carbon emissions from a natural fuel source. However, exploration of natural H_2 accumulations remains limited. Thus, we present the first long-term, multi-gas monitoring of a natural H_2 seep in Australia.

H_2 emissions occurred in significant concentrations, varied in amplitude across seasons and occurred as diurnal emissions with irregular high-concentration pulses. We interpret that H_2 micro-seepage was controlled by pressure pumping and soil moisture. The large pulses are interpreted to be the result of the H_2 gas pressure overcoming the interfacial tension of groundwater resulting in a sudden release.

H_2 emissions were inhibited by long-term high groundwater levels, which indicates that groundwater at ambient temperatures and pressures can form a barrier to the upward flow of H_2 gas through the soil profile and inhibit the soil gas H_2 readings at the surface.

This work has significant implications for natural H_2 exploration using soil gas monitoring techniques. False negatives are possible and likely in areas subject to inundation. When conducting soil gas sampling it is preferable to operate during the dry season and groundwater levels need to be considered, particularly in low-lying areas. Novel exploration methods will be required in wet environments.

Our confirmation of natural H_2 seepage on the Yilgarn Craton indicates active H_2 generation in the subsurface. The fundamental information on natural H_2 seepage provided by this study de-risks H_2 exploration in Western Australia, thus aiding in the implementation of a hydrogen economy.

Acknowledgments

The WHALI and EVA units providing autonomous monitoring measurements were developed by Axiom Sensing Pty Ltd and used with permission from Axiom Sensing Pty Ltd. The authors are grateful to Hayden Long, Ted Atkinson, Alex Vouyoucalos, Brent Spiers and Michael Atkinson for their assistance in the field. The FF4 site is located on private property and the authors would like to thank Mr M.Brennan and later Mr R. Fields for allowing access to the site over three years.

Funding

This research is jointly supported by the CSIRO iPhD Scholarship in collaboration with Gold Hydrogen Ltd. The sponsors played no role in the design, analysis, or reporting of this study.

We would also like to thank the Australian Research Council for financial support (ARC grant DP220102907), and Gehyra Flux Pty Ltd for financial support (G1006788).

Conflicts of interest

The authors declare no conflicts of interest.

Author contribution statement

All authors have read and agreed to the published version of the manuscript. K.D. was responsible for the project scope, design, and fieldwork. K.D. and E.F. were jointly responsible for writing the paper. S.I., A.K., L.E., and A.G. together were responsible for project conceptualization and editing of the manuscript.

References

1 Gielen D., Boshell F., Saygin D., Bazilian M.D., Wagner N., Gorini R. (2019) The role of renewable energy in the global energy transformation, *Energy Strat. Rev.* **24**, 38–50.
2 Fan L., Tu Z., Chan S.H. (2021) Recent development of hydrogen and fuel cell technologies: a review, *Energy Rep.* **7**, 8421–8446.
3 Bhattacharyya R., Singh K.K., Bhanja K., Grover R.B. (2024) Using electrolytic hydrogen production and energy storage for balancing a low carbon electricity grid: scenario assessments for India, *Energy Clim. Change* **5**, 100131.
4 Parente C., Teixeira F., Cerdeira J. (2024) Stakeholders' perceptions of hydrogen and reflections on energy transition governance, *Energy Sustain. Soc.* **14**, 1, 15.
5 Megía P.J., Vizcaíno A.J., Calles J.A., Carrero A. (2021) Hydrogen production technologies: from fossil fuels toward renewable sources. A mini review, *Energy Fuels* **35**, 20, 16403–16415.
6 Glenk G., Reichelstein S. (2019) Economics of converting renewable power to hydrogen, *Nat. Energy* **4**, 3, 216–222.
7 Dorn F.M. (2024) Towards a multi-color hydrogen production network? Competing imaginaries of development in northern Patagonia, Argentina, *Energy Res. Soc. Sci.* **110**, 103457.
8 Ishaq H., Dincer I., Crawford C. (2022) A review on hydrogen production and utilization: challenges and opportunities, *Int. J. Hyd. Energy* **47**, 62, 26238–26264.
9 Brandt A.R. (2023) Greenhouse gas intensity of natural hydrogen produced from subsurface geologic accumulations, *Joule* **7**, 8, 1818–1831.
10 Prinzhofer A., Tahara Cissé C.S., Diallo A.B. (2018) Discovery of a large accumulation of natural hydrogen in Bourakebougou (Mali), *Int. J. Hyd. Energy* **43**, 42, 19315–19326.
11 Boschee P. (2023) Comments: the new "Gold Rush" hunts for subsurface hydrogen, *J. Petrol. Technol.* **75**, 11, 10–11.
12 Gold H. (2023) Ramsay 2 update, in: *Very High Hydrogen Concentrations up to 86% Purity Found Along with the*

Very High Helium Concentrations, Australian Stock Exchange.
13 Stalker L., Talukder A., Strand J., Josh M., Faiz M. (2022) Gold (hydrogen) rush: risks and uncertainties in exploring for naturally occurring hydrogen, *APPEA J.* **62**, 361–380.
14 Moretti I., Geymond U., Pasquet G., Aimar L., Rabaute A. (2022) Natural hydrogen emanations in Namibia: field acquisition and vegetation indexes from multispectral satellite image analysis, *Int. J. Hyd. Energy* **47**, 84, 35588–35607.
15 Moretti I., Brouilly E., Loiseau K., Prinzhofer A., Deville E. (2021) Hydrogen emanations in intracratonic areas: new guide lines for early exploration basin screening, *Geosciences* **11**, 3, 145.
16 Lévy D., Roche V., Pasquet G., Combaudon V., Geymond U., Loiseau K., Moretti I. (2023) Natural H 2 exploration: tools and workflows to characterize a play, *Sci. Technol. Energy Trans.* **78**, 27.
17 Zgonnik V. (2020) The occurrence and geoscience of natural hydrogen: a comprehensive review, *Earth-Sci. Rev.* **203**, 103140.
18 Frery E., Langhi L., Maison M., Moretti I. (2021) Natural hydrogen seeps identified in the North Perth Basin, Western Australia, *Int. J. Hyd. Energy* **46**, 61, 31158–31173.
19 Mainson M., Heath C., Pejcic B., Frery E. (2022) Sensing hydrogen seeps in the subsurface for natural hydrogen exploration, *Appl. Sci.* **12**, 13, 6383.
20 Prinzhofer A., Moretti I., Francolin J., Pacheco C., D'Agostino A., Werly J., Rupin F. (2019) Natural hydrogen continuous emission from sedimentary basins: the example of a Brazilian H2-emitting structure, *Int. J. Hyd. Energy* **44**, 5676–5685.
21 Moretti I., Prinzhofer A., Françolin J., Pacheco C., Rosanne M., Rupin F., Mertens J. (2021) Long-term monitoring of natural hydrogen superficial emissions in a brazilian cratonic environment. Sporadic large pulses versus daily periodic emissions, *Int. J. Hyd. Energy* **46**, 5, 3615–3628.
22 Cathles L., Prinzhofer A. (2020) What pulsating H2 emissions suggest about the H2 resource in the Sao Francisco Basin of Brazil, *Geosciences* **10**, 149.
23 Aimar L., Frery E., Strand J., Heath C., Khan S., Moretti I., Ong C. (2023) Natural hydrogen seeps or salt lakes: how to make a difference? Grass Patch example, Western Australia, *Front. Earth Sci.* **11**, 14.
24 Zgonnik V., Beaumont V., Deville E., Larin N., Pillot D., Farrell K.M. (2015) Evidence for natural molecular hydrogen seepage associated with Carolina bays (surficial, ovoid depressions on the Atlantic Coastal Plain, Province of the USA), *Prog. Earth Planet. Sci.* **2**, 1, 31.
25 Smithies R.H., Witt W.K. (1997) Distinct basement terranes identified from granite geochemistry in late Archaean granite-greenstones, Yilgarn Craton, Western Australia, *Precambr. Res.* **83**, 185–201.
26 Rowe M., Kemp A., Wingate M., Petersson A., Whitehouse M., Riet C. (2022) Cratonisation of Archaean continental crust: insights from U-Pb zircon geochronology and geochemistry of granitic rocks in the Narryer Terrane, northwest Yilgarn Craton, *Precambr. Res.* **372**, 106609.
27 Tucker N., Hammerli J., Kemp A., Rowe M., Gray C., Jeon H., Whitehouse M., Roberts M. (2024) Ultrahigh thermal gradient granulites in the Narryer Terrane, Yilgarn Craton, Western Australia, provide a window into the composition and formation of Archean lower crust, *J. Metamorph. Geol.* **42**, 4, 425–470.
28 Chen S., Riganti A., Wyche S., Greenfield J., Nelson D. (2003) Lithostratigraphy and tectonic evolution of contrasting greenstone successions in the central Yilgarn Craton, Western Australia, *Precambr. Res.* **127**, 249–266.
29 Bourne B., Trench A., Dentith M., Ridley J. (1993) Physical property variations within Archaean granite-greenstone Terrane of the Yilgarn Craton, Western Australia: the influence of metamorphic grade, *Explor. Geophys.* **24**, 4, 367–374.
30 Calvert A.J., Doublier M.P. (2018) Archaean continental spreading inferred from seismic images of the Yilgarn Craton, *Nat. Geosci.* **11**, 7, 526–530.
31 Swager C., Goleby B., Drummond B.J., Rattenbury M.S., Williams P.R. (1997) Crustal structure of granite-greenstone terranes in the Eastern Goldfields, Yilgarn Craton, as revealed by seismic reflection profiling, *Precambrian Res.* **83**, 43–56.
32 Anand R.R., Paine M. (2002) Regolith geology of the Yilgarn Craton, Western Australia: implications for exploration, *Aust. J. Earth Sci.* **49**, 1, 3–162.
33 Mulder J.A., Nebel O., Gardiner N.J., Cawood P.A., Wainwright A.N., Ivanic T.J. (2021) Crustal rejuvenation stabilised Earth's first cratons, *Nat. Commun.* **12**, 1, 3535.
34 Deshon M. (2001) Groundwater study of the Wongan Hills townsite, in: *Resource management technical reports.* Department of Primary Industries and Regional Development, Western Australia, p. 38.
35 Davies K., Esteban L., Keshavarz A., Iglaeur S. (2024) Advancing natural hydrogen exploration: headspace gas analysis in water-logged environments, *Energy Fuels* **38**, 2010–2017.
36 Halas P., Dupuy A., Franceschi M., Bordmann V., Fleury J.-M., Duclerc D. (2021) Hydrogen gas in circular depressions in South Gironde, France: flux, stock, or artefact?, *Appl. Geochem.* **127**, 104928.
37 Air-met S. (2012) *GA5000 portable gas analyser landfill & contaminated land specification sheet*, Air-Met Scientific Pty Ltd., p. 4. https://www.airmet.com.au/assets/documents/product/301/GA5000-Datasheet.pdf.
38 Industrial S. (2019) Gas detection and monitoring solutions iBrid MX6 product specifications, in: *Internal Report*, I. Scientific, Editor. Industrial Scientific, p. 51. https://www.indsci.com/en/.
39 SGX. (2009) *EC4-100-H2S hydrogen sulfide electrochemical sensor*, S.S. Ltd, Editor, p. 2.
40 SGX. (2009) *EC4-1000-H2 hydrogen electrochemical sensor*, S.S. Ltd, Editor, p. 2.
41 SGX. (2018) *Integrated IR datasheet*, S.S.I. Ltd, Editor, p. 9.
42 Suleimenov O.M., Krupp R.E. (1994) Solubility of hydrogen sulfide in pure water and in NaCl solutions, from 20 to 320°C and at saturation pressures, *Geochim. Cosmochim. Acta* **58**, 11, 2433–2444.
43 Laemmel T., Mohr M., Schack-Kirchner H., Schindler D., Maier M. (2017) Direct observation of wind-induced pressure-pumping on gas transport in soil, *Soil Sci. Soc. Am. J.* **81**, 4, 770–774.
44 Laemmel T., Mohr M., Longdoz B., Schack-Kirchner H., Lang F., Schindler D., Maier M. (2019) From above the forest into the soil – how wind affects soil gas transport through air pressure fluctuations, *Agric. For. Meteorol.* **265**, 424–434.

45 Massman W.J., Frank J.M. (2022) Modeling gas flow velocities in soils induced by variations in surface pressure, heat, and moisture dynamics, *J. Adv. Model. Earth Syst.* **14**, 10, e2022MS003086.

46 Bahlmann L.M., Smits K.M., Heck K., Coltman E., Helmig R., Neuweiler I. (2020) Gas component transport across the soil-atmosphere interface for gases of different density: experiments and modeling, *Water Resour. Res.* **56**, 9, e2020WR027600.

47 Buckingham E. (1904) *Contributions to our knowledge of the aeration of soils.* U.S. Dept. of Agriculture, Bureau of Soils, Washington, D.C.

48 Su Z., Wu B., Gong Y. (2015) Determination of gas diffusion coefficient in soils with different porosities, *Nongye Gongcheng Xuebao/Trans. Chin. Soc. Agric. Eng.* **31**, 108–113.

49 Neira J., Ortiz M., Morales L., Acevedo E. (2015) Oxygen diffusion in soils: understanding the factors and processes needed for modeling, *Chilean J. Agric. Res.* **75**, 35–44.

50 Etiope G., Martinelli G. (2002) Migration of carrier and trace gases in the geosphere: an overview, *Phys. Earth Planet. Interiors* **129**, 3, 185–204.

51 Forde O.N., Cahill A.G., Beckie R.D., Mayer K.U. (2019) Barometric-pumping controls fugitive gas emissions from a vadose zone natural gas release, *Sci. Rep.* **9**, 1, 14080.

52 Cheng Q., Zhang M., Jin H., Ren Y. (2022) Spatiotemporal variation characteristics of hourly soil temperature in different layers in the low-latitude plateau of China, *Front. Environ. Sci.* **10**, 1091985.

53 Horton B., Corkrey R. (2011) A weighted coefficient model for estimation of Australian daily soil temperature at depths of 5 cm to 100 cm based on air temperature and rainfall, *Soil Res.* **49**, 305–314.

54 Zeng Y., Su Z., Wan L., Yang Z., Zhang T., Tian H., Shi X., Wang X., Cao W. (2009) Diurnal pattern of the drying front in desert and its application for determining the effective infiltration, *Hydrol. Earth Syst. Sci.* **13**, 6, 703–714.

55 Pan B., Yin X., Ju Y., Iglauer S. (2021) Underground hydrogen storage: influencing parameters and future outlook, *Adv. Colloid Interface Sci.* **294**, 102473.

56 Simon J., Fulton P., Prinzhofer A., Cathles L. (2020) Earth tides and H2 venting in the Sao Francisco Basin, Brazil, *Geosciences* **10**, 414.

57 Myagkiy A., Brunet F., Popov C., Krüger R., Guimarães H., Sousa R.S., Charlet L., Moretti I. (2020) H2 dynamics in the soil of a H2-emitting zone (São Francisco Basin, Brazil): Microbial uptake quantification and reactive transport modelling, *Appl. Geochem.* **112**, 104474.

58 Beaubien S., Ruggiero L., Annunziatellis A., Bigi S., Ciotoli G., Deiana P., Graziani S., Lombardi S., Tartarello Maria C. (2014) The importance of baseline surveys of near-surface gas geochemistry for CCS monitoring, as shown from onshore case studies in Northern and Southern Europe, *Oil Gas Sci. Technol.* **70**, 4, 615–633.

59 Beaubien S.E., et al. (2013) Monitoring of near-surface gas geochemistry at the Weyburn, Canada, CO2-EOR site, 2001–2011, *Int. J. Greenhouse Gas Control* **16**, S236–S262.

60 Jones D.G., Barlow T., Beaubien S.E., Ciotoli G., Lister T. R., Lombardi S., May F., Möller I., Pearce J.M., Shaw R.A. (2009) New and established techniques for surface gas monitoring at onshore CO2 storage sites, *Energy Proc.* **1**, 1, 2127–2134.

61 Salmawati S., Sasaki K., Sugai Y., Nguele R. (2018) Characterization of natural soil CO2 flux: implication for leakage detection monitoring at CO2 geological sites, *SSRN Electr. J.* **GHGT-14**, 6.

62 Salmawati S., Sasaki K., Sugai Y., Yousefi-Sahzabi A. (2019) Estimating a baseline of soil CO2 flux at CO2 geological storage sites, *Environ. Monit. Assess.* **191**, 9, 1–12.

63 Carman C.H., Locke Ii R.A., Blakley C.S. (2014) Update on soil CO2 flux monitoring at the Illinois Basin – Decatur Project, USA, *Energy Proc.* **63**, 3869–3880.

64 Reimer G.M. (1979) The use of soil-gas helium concentrations for earthquake prediction: studies of factors causing diurnal variation, in: *Open-File Report.*

65 Camarda M., De Gregorio S., Capasso G., Di Martino R.M. R., Gurrieri S., Prano V. (2019) The monitoring of natural soil CO2 emissions: issues and perspectives, *Earth-Sci. Rev.* **198**, 102928.

66 Iglauer S., Ali M., Keshavarz A. (2020) Hydrogen wettability of sandstone reservoirs: implications for hydrogen geostorage, *Geophys. Res. Lett.* **48**, 3, 90814.

67 Strauch B., Pilz P., Hierold J., Zimmer M. (2023) Experimental simulations of hydrogen migration through potential storage rocks, *Int. J. Hyd. Energy* **48**, 66, 25808–25820.

68 Lodhia B.H., Peeters L. (2024) The migration of hydrogen in sedimentary basins, *Aust. Energy Prod. J.* **64**, 1, 186–194.

69 Salmawati S., Sasaki K., Sugai Y., Nguele R. (2018) Characterization of natural soil CO2 flux: implication for leakage detection monitoring at CO2 geological sites, in: *GHGT-14*, Melbourne, p. 6.

70 Schlömer S., Möller I., Furche M. (2014) Baseline soil gas measurements as part of a monitoring concept above a projected CO2 injection formation—a case study from Northern Germany, *Int. J. Greenhouse Gas Control* **20**, 57–72.

71 Verstraeten W.W., Veroustraete F., Feyen J. (2008) Assessment of evapotranspiration and soil moisture content across different scales of observation, *Sensors (Basel)* **8**, 1, 70–117.

72 Wang H., Zhao R., Zhao D., Liu S., Fu J., Zhang Y., Dai N., Song D., Ding H. (2022) Microbial-mediated emissions of greenhouse gas from farmland soils: a review, *Processes* **10**, 11, 14.

73 Boreham C.J., Edwards D.S., Czado K., Rollet N., Wang L., van der Wielen S., Champion D., Blewett R., Feitz A., Henson P.A. (2021) Hydrogen in Australian natural gas: occurrences, sources and resources, *APPEA J.* **61**, 1, 163–191.

74 Larin N., Zgonnik V., Rodina S., Deville E., Prinzhofer A., Larin V.N. (2015) Natural molecular hydrogen seepage associated with surficial, rounded depressions on the European Craton in Russia, *Nat. Resour. Res.* **24**, 3, 369–383.

75 Bourdet J., et al. (2023) Natural hydrogen in low temperature geofluids in a Precambrian granite, South Australia. Implications for hydrogen generation and movement in the upper crust, *Chem. Geol.* **638**, 121698.

76 Zhao M., Wang M., Zhao Y., Hu N., Qin L., Ren Z., Wang G., Jiang M. (2022) Soil microbial abundance was more affected by soil depth than the altitude in peatlands, *Front. Microbiol.* **13**, 1068540.

77 Su X., Zhao W., Xia D. (2018) The diversity of hydrogen-producing bacteria and methanogens within an in situ coal seam, *Biotechnol. Biofuels* **11**, 1, 245.

78 Hao J., Chai Y.N., Lopes L.D., Ordóñez R.A., Wright E.E., Archontoulis S., Schachtman D.P. (2021) The effects of soil depth on the structure of microbial communities in agricultural soils in Iowa, USA, *Appl. Environ. Microbiol.* **87**, 4, e02673-20.

79 Pimentel M., Mathur R., Chang C. (2013) Gas and the microbiome, *Curr. Gastroenterol. Rep.* **15**, 12, 356.

80 Pander B., Mortimer Z., Woods C., McGregor C., Dempster A., Thomas L., Maliepaard J., Mansfield R., Rowe P., Krabben P. (2020) Hydrogen oxidising bacteria for production of single-cell protein and other food and feed ingredients, *Eng. Biol.* **4**, 2, 21–24.

81 Sinha P., Roy S., Das D. (2015) Role of formate hydrogen lyase complex in hydrogen production in facultative anaerobes, *Int. J. Hyd. Energy* **40**, 29, 8806–8815.

82 Lee H.-S., Vermaas W.F.J., Rittmann B.E. (2010) Biological hydrogen production: prospects and challenges, *Trends Biotechnol.* **28**, 5, 262–271.

83 Marriott R.A., Pirzadeh P., Marrugo-Hernandez J.J., Raval S. (2016) Hydrogen sulfide formation in oil and gas, *Can. J. Chem.* **94**, 4, 406–413.

84 Marshall D., Downes P.J., Ellis S., Greene R., Loughrey L., Jones P. (2016) Pressure–temperature–fluid constraints for the Poona Emerald deposits, Western Australia: fluid inclusion and stable isotope studies, *MDPI Min.* **6**, 4, 22.

85 Nelson D.R. (1997) Evolution of the Archaean granite-greenstone terranes of the Eastern Goldfields, Western Australia: SHRIMP U.Pb zircon constraints, *Precambrian Res.* **83**, 1, 57–81.

86 Pidgeon R.T., Wilde S.A., Compston W., Shield M.W. (1990) Archaean evolution of the Wongan Hills Greenstone Belt, Yilgarn Craton, Western Australia, *Aust. J. Earth Sci.* **37**, 3, 279–292.

87 Hosgörmez H. (2007) Origin of the natural gas seep of Çirali (Chimera), Turkey: site of the first Olympic fire, *J. Asian Earth Sci.* **30**, 1, 131–141.

88 Abrajano T.A., Sturchio N.C., Bohlke J.K., Lyon G.L., Poreda R.J., Stevens C.M. (1988) Methane-hydrogen gas seeps, Zambales Ophiolite, Philippines: deep or shallow origin?, *Chem. Geol.* **71**, 1, 211–222.

89 Deville E., Prinzhofer A. (2016) The origin of N2-H2-CH4-rich natural gas seepages in ophiolitic context: a major and noble gases study of fluid seepages in New Caledonia, *Chem. Geol.* **440**, 139–147.

90 Kelley D.S., et al. (2005) A serpentinite-hosted ecosystem: the lost city hydrothermal field, *Science* **307**, 5714, 1428–1434.

91 Brazelton W.J., Morrill P.L., Szponar N., Schrenk M.O. (2013) Bacterial communities associated with subsurface geochemical processes in continental serpentinite springs, *Appl. Environ. Microbiol.* **79**, 13, 3906–3916.

92 Dodd M.S., et al. (2022) Abiotic anoxic iron oxidation, formation of Archean banded iron formations, and the oxidation of early Earth, *Earth Planet. Sci. Lett.* **584**, 117469.

93 Marty B. (2011) Mantle volatiles, in: *Encyclopedia of astrobiology*, M. Gargaud, et al., Editors, Springer Berlin Heidelberg, Berlin, Heidelberg, pp. 959–960.

94 Sutton J., Tamar E. (2014) One hundred volatile years of volcanic gas studies at the Hawaiian Volcano Observatory, in: *Characteristics of Hawaiian Volcanoes*, M. Poland, T.J. Takahashi, C. Landowski, Editors, United States Geological Survey: U.S. Geological Survey Professional Paper 1801, pp. 295–320.

95 Marty B., Tolstikhin I.N. (1998) CO2 fluxes from mid-ocean ridges, arcs and plumes, *Chem. Geol.* **145**, 3, 233–248.

96 Konn C., Charlou J.L., Holm N.G., Mousis O. (2015) The production of methane, hydrogen, and organic compounds in ultramafic-hosted hydrothermal vents of the Mid-Atlantic Ridge, *Astrobiology* **15**, 5, 381–399.

97 Zhou X., Shen Y., Zhang H., Song C., Li J., Liu Y. (2015) Hydrochemistry of the natural low pH groundwater in the coastal aquifers near Beihai, China, *J. Ocean Univ. China* **14**, 3, 475–483.

98 Burton M., Sawyer G., Granieri D. (2013) Deep carbon emissions from Volcanoes, *Rev. Mineral. Geochem.* **75**, 323–354.

99 Yonemura S., Yokozawa M., Shirato Y., Nishimura S., Nouchi I. (2009) Soil CO2 concentrations and their implications in conventional and no-tillage agricultural fields, *J. Agric. Meteorol.* **65**, 141–149.

100 Parnell J., Blamey N. (2017) Global hydrogen reservoirs in basement and basins, *Geochem. Trans.* **18**, 1, 2.

101 Mavrogenes J.A., Bodnar R.J. (1994) Hydrogen movement into and out of fluid inclusions in quartz: experimental evidence and geologic implications, *Geochim. Cosmochim. Acta* **58**, 1, 141–148.

102 Goscombe B., Foster D.A., Blewett R., Czarnota K., Wade B., Groenewald B., Gray D. (2019) Neoarchaean metamorphic evolution of the Yilgarn Craton: a record of subduction, accretion, extension and lithospheric delamination, *Precambrian Res.* **335**, 105441.

103 Dentith M., Aitken A., Evans S., Joly A. (2013) Regional mineral exploration targeting for gold and nickel deposits using crustal electrical conductivity variations determined using the magnetotelluric method, in: *ASEG Extended Abstracts*, p. 1.

104 Reading A., Kennett B., Dentith M. (2003) Seismic structure of the Yilgarn Craton, Western Australia, *Aust. J. Earth Sci.* **50**, 427–438.

105 Weber U.D., Kohn B.P., Gleadow A.J.W., Nelson D.R. (2005) Low temperature Phanerozoic history of the Northern Yilgarn Craton, Western Australia, *Tectonophysics* **400**, 1, 127–151.

106 Warr O., Giunta T., Ballentine C.J., Sherwood Lollar B. (2019) Mechanisms and rates of 4He, 40Ar, and H2 production and accumulation in fracture fluids in Precambrian Shield environments, *Chem. Geol.* **530**, 119322.

107 Bouquet A., Glein C.R., Wyrick D., Waite J.H. (2017) Alternative energy: production of H2 by radiolysis of water in the Rocky Cores of icy bodies, *Astrophys. J. Lett.* **840**, 1, L8.

108 Donze F., Truche L., Namin P., Lefeuvre N., Bazarkina E. (2020) Migration of natural hydrogen from deep-seated sources in the São Francisco Basin, Brazil, *Geosciences* **10**, 16.

109 Dzaugis M.E., Spivack A.J., Dunlea A.G., Murray R.W., D'Hondt S. (2016) Radiolytic hydrogen production in the subseafloor basaltic aquifer, *Front. Microbiol.* **7**, 76.

110 Milkov A.V. (2022) Molecular hydrogen in surface and subsurface natural gases: abundance, origins and ideas for deliberate exploration, *Earth-Sci. Rev.* **230**, 104063.

111 Liao D., Feng D., Luo J., Yun X. (2023) Relationship between radiogenic heat production in granitic rocks and emplacement age, *Energy Geosci.* **4**, 4, 100157.

112 Cullen R. (2023) Exploration update september 2023, in: *ASZ Release*, C.R.P. Ltd, Editor, p. 17.

113 Bepari M.I., Meesungnoen J., Jay-Gerin J.-P. (2023) Early and transient formation of highly acidic pH spikes in water radiolysis under the combined effect of high dose rate and high linear energy transfer, *Radiation* **3**, 3, 165–182.